AIAA JOURNAL
Vol. 49, No. 2, February 2011

Experimental Investigation of the Unstart Process of a Generic Hypersonic Inlet

Hui-jun Tan,* Liu-gang Li,† Yu-fen Wen,† and Qi-fan Zhang†
Nanjing University of Aeronautics and Astronautics, 210016 Nanjing, People's Republic of China

DOI: 10.2514/1.J050200

To provide information for the detection, prediction, and control of the inlet unstart, the entire process from a started status to an unstarted status of a generic two-dimensional hypersonic inlet is studied experimentally at Mach 5. The movement of a flow plug at the exit of the duct is used to gradually increase the throttling to simulate the unstart process caused by the excessive heat release in the combustor. Simultaneous high-speed schlieren imaging and dynamic surface pressure measurements are used to record the unsteady flow structures and surface pressures of the unstart process. According to the internal and external flows, the unstart process can be divided into four stages, namely, shock train in the combustor, shock train in the isolator, separation bubble in the throat, and unstart. The transient flow patterns of each stage are substantially different and the corresponding dynamics pressures also have prominent time-frequency features, which make the detection and prediction of the inlet unstart based on dynamic pressures possible. Since the sensor placed at the end of the top surface of the inlet contract part, marked by C1, obtains the most abundant time-frequency characteristics which can be used to discern the different stages of the inlet unstart process, the location where it stays is regarded as the first choice for sensor placement to construct a practical inlet-status-monitoring system.

I. Introduction

UNSTART is an abnormal operating state for hypersonic inlets. In general, when the airflow capture characteristic of a hypersonic inlet is not altered by the internal flow field, it is regarded as operating in a started mode, otherwise in an unstarted condition [1]. Experiences show that the undesired unstart phenomenon may lead to violent shock system oscillations, prominent pressure fluctuations, and abrupt performance reductions which result in the substantial engine thrust loss and even the combustor flameout [2,3]. The caused unsteady aerodynamic and thermal loads [4] can even lead to the destruction of the engine and the failure of the flight control. Therefore, the unstart phenomenon should be avoided at any time for proper operation. However, it is difficult to avoid inlet unstart in practice since it may result from various factors, such as large internal contractions, strong shock/boundary-layer interactions, low operating Mach numbers, large flight angles of attack, improper fuel regulations, excessive combustor pressures, perturbations from the takeover action of the propulsion system, disturbances of the operating mode transition of the scramjet, even the atmosphere parameter fluctuations, etc. What's more, due to the immaturity of design methods for hypersonic inlets, the inaccuracy of computational fluid dynamics tools for hypersonic flows, and the inconsistency of ground simulated conditions with flight conditions, the unstarted state of hypersonic inlets is inevitable during the development of hypersonic airbreathing propulsion systems. In the flight test for a scramjet with a designed operating Mach number range of 3.5 to 6.5, which was carried out jointly by the Central Institute of Aviation Motors and NASA in 1998, the unstart phenomenon of the hypersonic inlet led to a partial unfulfillment of the scheduled flight task. Subsequent analysis reported by Voland et al. [5] indicates that the inlet started at Mach 3.5, but was soon unstarted due to the over fueling in the combustor. After about 12 s, the flight Mach number reached 5.0 and the inlet restarted. However, the inlet controlling system still sensed that the inlet was unstarted. Hence, the first stage fueling was never opened during the entire flight test. Also, in the joint scramjet flight test, which was named as HyCAUSE and performed by the Defense Advanced Research Projects Agency and Queensland in 2007, the unstart phenomenon of the inward turning inlet emerged periodically and partially contributed to the absence of hydrogen combustion in the combustor [6]. Therefore, in recent years the unstart issue of hypersonic inlets has generated a lot of research interest [3,7–9]. Aiming to provide the underlying transient flow mechanism and the unsteady pressure behaviors for the detection, prediction, and control of the inlet unstart, the current paper involves experimental investigations of the entire unstart process of a generic two-dimensional hypersonic inlet.

II. Literature Review

Unstart phenomenon also exists for supersonic inlets. The related unsteady flow pattern and oscillatory mechanism of supersonic inlet unstart are more or less clear from numerous numerical and experimental studies made in the past decades [10–13]. For supersonic inlets, the unstart phenomenon may exhibit two different oscillatory phases, of similar frequencies but different amplitudes, called "little buzz" and "big buzz." As inlet buzz is a self-excited flow in essence, there exists a feedback loop of signals in which the acoustic wave often plays the role of upstream feedback. Hence the base frequency and other energy-containing frequencies of supersonic inlet buzz are often closely related to the acoustic resonant modes of the duct. However, the flow pattern in unstarted hypersonic inlets is quite different from that of supersonic inlets since the airflow is spilled supersonically for hypersonic inlets but subsonically for supersonic inlets, as reported by Curran and Murthy [1]. Therefore the achievements made in supersonic inlet buzz can not be applied to hypersonic inlets directly. As a result, a number of numerical and experimental studies were performed to reveal the flow patterns of unstarted hypersonic inlets [3,7,8,14–16]. Experimental studies on a generic two-dimensional scramjet inlet by Scott [14] made use of a rapidly driven plug at the duct exit to initiate unstart. The unstart phenomenon was recorded using a schlieren system and a camera. But the framing rate and the shutter speed of the camera were too slow to fully capture the dynamics of unstart. Rodi et al. [15] investigated the unstart phenomenon in a two-dimensional inlet of a dual-mode, ramjet/scramjet configuration. The mean and time-accurate pressures were measured both under back pressure-induced

Received 9 September 2009; revision received 26 August 2010; accepted for publication 29 October 2010.

*Professor, College of Energy and Power Engineering.
†Graduate Student, College of Energy and Power Engineering.

unstarted conditions and under cowl-induced unstarted conditions. The pressure unsteadiness caused by the unstarted flow was noticed, but due to the insufficiency of dynamic pressure gauges and the lack of flow visualization, the unsteady flow patterns of hypersonic inlets were still obscure. For some cases, it was not very clear whether the unsteady behavior of the recorded pressure signal is the result of noisy measurements or not. Shimura et al. [16] investigated the unstart phenomenon of a sidewall compression inlet which was installed in a combusting scramjet model. Unstart of the inlet was induced by the excessive hydrogen injection. During the unstarted phase, the inlet surface pressures showed violent oscillations and the peak pressures on the sidewall were found more than two times greater than those of started conditions. The authors also suggested that the inlet unstart could be detected with pressure sensors flush-mounted on the sidewall. Tan and Guo [3] investigated the unsteady flows of an unstarted three-dimensional hypersonic inlet for dual-combustor ramjets. Violent oscillations of the external shock system and the instantaneous surface pressures were observed in their experiment. Tan et al. [7] experimentally investigated the unstarted flows in a rectangular hypersonic inlet at a free stream Mach number of 5. High-speed schlieren imaging and time-accurate pressure measurements were used to depict the external/internal flow structures and the unsteady behaviors of surface pressures. The observed oscillatory flows of hypersonic inlet unstart were classified into little buzz and big buzz. The authors also mentioned that traditional oscillation mechanism based on acoustic wave feedback loop for supersonic inlet was invalid for hypersonic inlet buzz since large transient supersonic region existed in a buzz cycle. Thus a new oscillation mechanism was brought forward. Wagner et al. [8] investigated experimentally the unstart dynamics of a simplified inlet/isolator model in a Mach 5 flow. Unstart was initiated by deflecting a flap at the exit plane of the isolator. The upstream propagation of the unstart shock system was recorded and analyzed. The unstart time scales and the unstarted flow structure showed little relations with the flap rise time which varied from 140 to 530 ms. Three types of unstarted flows, namely, high-amplitude oscillatory unstarted flow, nonoscillatory unstarted flow, and low-amplitude oscillatory unstarted flow, were observed.

To provide the capability of unstart control for hypersonic inlets, the detection and prediction of unstart were concerned in several papers [5,9,17,18]. Hawkins and Marquart [17] suggested three techniques for the unstart detection of a two-dimensional generic supersonic/hypersonic inlet, which were based on internal flow visualizations, steady-state pressure relations, and dynamic pressure-time histories, respectively. The flow visualization technique was found to be the most positive and reliable unstart detection technique. However, it was not practical for any flight test and any future hypersonic vehicles due to the requirement of the complex schlieren system. The second technique based on steady-state pressure relations was much more realizable, but the unstart detection criterion varied with the inlet designs, the flight conditions, and even the size of the separation bubble near the throat. Thus, misjudgment might occur while the actual flow pattern slightly deviated from the assumed one. In [5], the second technique was used according to the steady-state pressure ratio of the inlet throat, which mistook the inlet restarted condition for an unstarted condition. It was later found out that the misjudgment was caused by a boundary-layer separation near the throat which was larger than anticipated. To improve the accuracy of the second unstart detection technique, Yu et al. [9] introduced the support vector machine-recursive feature elimination algorithm to obtain the optimal classification criteria of inlet start/unstart. An isolated belt was formed between the start and unstart boundaries in their newly developed classification criterion. The third technique suggested in [17] was built upon surface dynamic pressures and advanced time-frequency analysis methods. This technique had the advantage that the unstart detection criterion was basically independent on the steady-state pressure relations and might be universal for different inlet designs. Another advantage of this technique was that it provided a real-time detection of unstart. It was also expected to predict the inlet unstart in advance. This technique was employed by Trapier et al. [18] to detect the buzz phenomenon and to predict its onset for a mixed-compression supersonic inlet with an operating Mach number range of 2 to 3. The precursor phenomena were observed several tenths of seconds before the onset of buzz. Thus two change-detection algorithms (cumulative sum and generalized likelihood ratio) were introduced to detect these precursors.

The preceding discussion shows that although substantial work has been done to improve the understanding of the unstart phenomenon of hypersonic inlets, much still remains unknown about the unstart dynamics. Few papers involve the transitional flow patterns and the unsteady surface pressures of the unstart process which are critical to the development of detection, prediction, and control methods for unstart. The current paper deals with the entire process from a started status to an unstarted status of a generic two-dimensional hypersonic inlet experimentally. Simultaneous high-speed schlieren imaging and dynamic surface pressure measurements were used to characterize the flow structures and the surface pressures of the unstart process.

III. Experimental Setup

A. Description of the Test Model

The test model simulates the full flowpath of a generic rectangular scramjet engine which consists of an inlet, an isolator, and a dump combustor (Fig. 1). The inlet is designed for a shock-on-lip Mach number of 6.0 and for a starting Mach number of 4.0. The external compression of the inlet is achieved by two ramps inclined by 10 and 21 deg to the freestream flow direction, respectively. The flow turning angle at the internal cowl is 13 deg. The total area contraction ratio of the inlet is 6.4 and the internal one is 2.2. Immediately after the inlet throat, a duct having constant cross section (100 mm in length and 10.5 mm in height) is provided which acts as an isolator. Downstream of the isolator is a simplified dump combustor with a length of 90 mm and a height of 16 mm. Two pieces of K9 glass are installed on the two sides of the duct, providing optical access to the internal flow field. A flow plug placed at the duct exit was driven by a linear electric motor to obtain different throttle ratios and the combustion-induced high pressures. A more complete description can be found in [7].

B. Experimental Conditions and Measurements

The experimental data are taken using a hypersonic wind tunnel at Nanjing University of Aeronautics and Astronautics. The facility runs in a blown-down mode with a usable runtime greater than 7 s. The wind tunnel air is supplied by two storage tanks with a volume of 40 m^3 at a pressure of 20 MPa. Tests can be conducted at plenum temperature of $400 \sim 650$ K and plenum pressure of $0.6 \sim 1.5$ MPa. The test chamber is fully closed with two embedded glass windows (300 mm in diameter) for optical access. Upstream the test chamber an interchangeable converging-diverging nozzle with an exit diameter of 500 mm is located, providing nominal freestream Mach

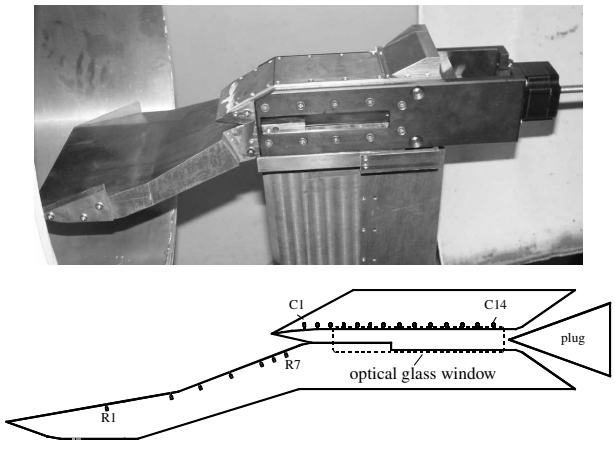

Fig. 1 Test model instrumented for simultaneous optical and pressure measurements.

Table 1 Test conditions for hypersonic inlet unstart

Property	Value
Nominal Mach no.	5.0
Actual Mach no.	4.92
Total temperature, K	580
Total pressure, 10^6 Pa	0.7
Usable runtime, s	>7
Diameter of the uniform flow region at the station of 300 mm downstream of the nozzle exit, mm	>300

numbers from 5.0 to 8.0 and flight conditions from 27 to 59 km. For the current experiment, the Mach 5 nozzle is used and the corresponding flow conditions are summarized in Table 1.

Time-accurate pressure measurements are performed by 21 fast-response pressure transducers to monitor the unsteady flow patterns in the test model. The transducers are flush-mounted in a row at the spanwise centerline of the model. The transducer locations are labeled R1–R7 (R1–R5: range of 100 kPa; R6–R7: range of 500 kPa, on the ramp) and C1–C14 (range of 500 kPa, on the cowl) on the schematic of Fig. 1. The transducer signals are each sent directly to the data acquisition system which consists of two National Instruments DAQ PCI-6115 cards, and are digitized at a rate of 20 kHz. According to the factory calibration data, the transducers have an accuracy of $\pm 0.1\%$ of the full range and a natural response frequency of 50 kHz. Practical use indicates that the total noise band of the electronics also adds an uncertainty (about 0.3 kPa for R1–R5 and 1.3 kPa for the others) to the instantaneous pressure values. During the test, the data sampling process is initiated before the wind tunnel starts and lasts 12 s to cover the entire operating process of the wind tunnel. The unsteady behaviors of the external and internal flow pattern are also recorded by CR2000 camera of Kodak, Inc. The sampling rate of the schlieren visualization is set 1000 frames per second for the current experiment. The corresponding sampling process can last only two seconds due to the memory limit. Therefore, the camera is triggered manually after the establishment of the flow field in the test model. The trigger signal is also recorded by the data acquisition system to obtain synchronization between the pressure data and imaging systems.

C. Test Procedure

For the current experiment, an increasing throttling ratio (TR) is formed by the continuously upstream movement of the flow plug to simulate the unstart process caused by the combustion-induced thermal choke. The TR is defined as

$$\mathrm{TR} = (1 - A_{\mathrm{th,plug}}/A_{\mathrm{combustor}}) \times 100\%$$

where $A_{\mathrm{th,plug}}$ is the throat area near the plug and $A_{\mathrm{combustor}}$ is the cross-sectional area of the combustor. The flow plug is placed at a rather downstream position, corresponding to a TR of 14%, to ensure an initial started condition for the inlet. While the internal flow field of the test model is established (about $t = 5770$ ms), the flow plug begins to move upstream at a velocity of 16 mm/s. The unstart phenomenon appears at about $t = 6220$ ms. While $t = 6800$ ms, the flow plug stops with a TR of 85%. Figure 2 shows the time sequence of the experiment according to the pressure-time history recorded by R3, for which zero on the time axis represents the start of the data sampling process.

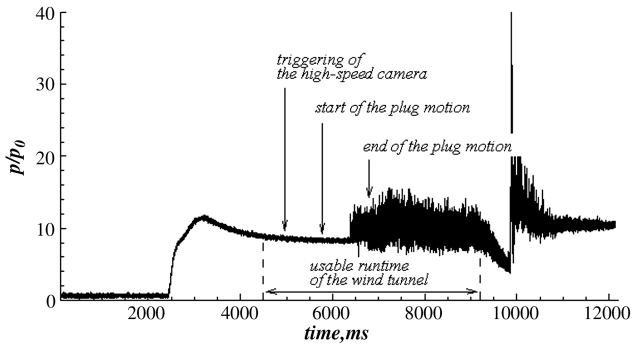

Fig. 2 Time sequence of the experiment.

IV. Results of the Unstart Process

Figure 3 presents the static pressure-time histories of typical survey points which are placed at the surface of the inlet throat, the isolator, and the combustor, respectively, during the entire unstart process. Every 20th point of the original data is plotted in Fig. 3 for clarity. As it can be seen, with the upstream movement of the flow plug the high pressure region in the duct extends and the time-averaged values increase. Finally, the pressure signals exhibit large-amplitude oscillations and the time-averaged values drop abruptly, indicating the emergence of unstart. The plug movement time before the unstart onset is 450 ms. According to the result obtained by Wagner et al. [8], the flap rise time hardly affects the unstart time scales and the unstarted flow structure. Thus the results obtained by the current experiment are representative. Based on the schlieren images and the pressure signals, the entire unstart process can be divided into four stages: a) shock train in the combustor, b) shock train in the isolator, c) separation bubble in the inlet throat, and d) unstart.

Since the surface pressure signals are nonstationary in nature, they can not be analyzed by traditional signal-processing methods such as the Fourier transform. Instead, time-frequency methods such as short-time Fourier transform or wavelet transform should be used to take into account the rapid changes of statistical properties (such as mean, rms amplitude, spectral content, etc.) in time. As compared with short-time Fourier transform, wavelet transform has the advantage that high resolution can be obtained both in time domain and in frequency domain by varying the length of wavelets. Therefore, wavelet transform is used in the current paper.

A. Shock Train in the Combustor (t < 5932 ms)

The shock train in ducts is a complex phenomenon that is frequently encountered in a supersonic pressure-gain process. It is characterized by strong shock/boundary-layer interactions, multiple successive normal or oblique shocks, a finite adverse pressure gradient in a finite flow region, and possible self-excited oscillation. The shock train appears in a variety of fluid devices such as

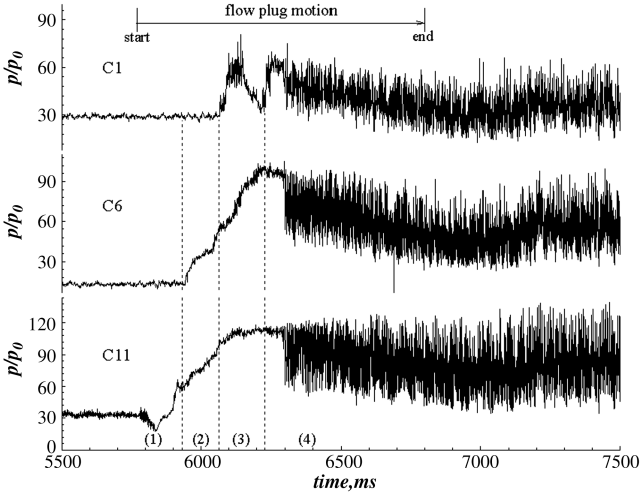

(1) Shock train in the combustor (t < 5932ms)
(2) Shock train in the isolator (t=5932ms-6064ms)
(3) Separation bubble in the throat (t=6064ms-6220ms)
(4) Unstart (t>6220ms)

Fig. 3 Static pressure-time histories of typical survey points during the unstart process.

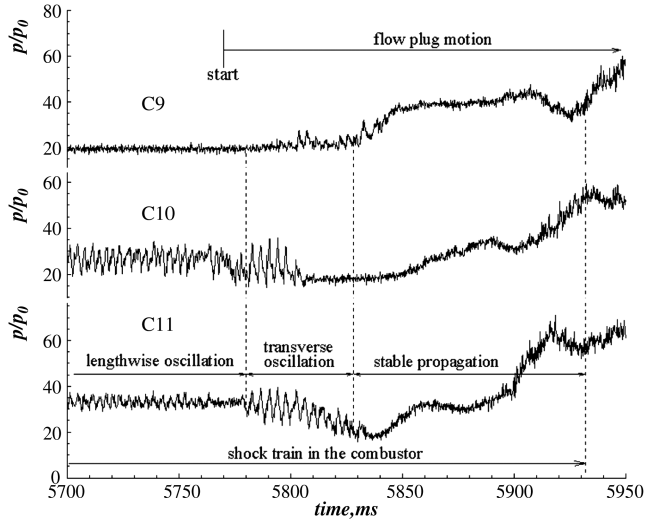

Fig. 4 Time slice of surface pressure signals of the stage of shock train in the combustor.

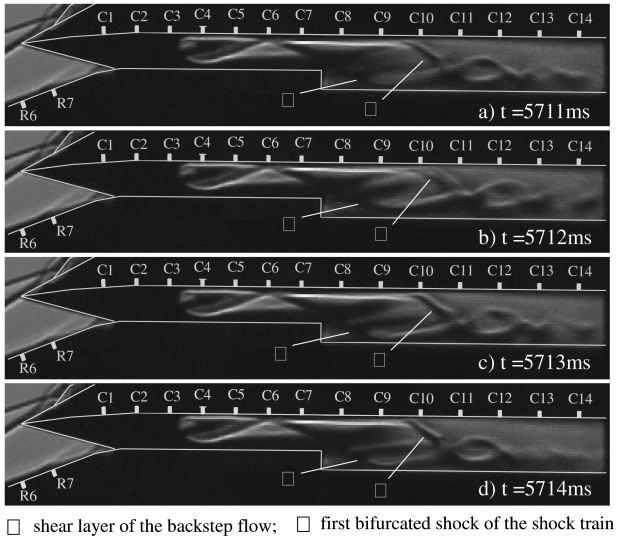

Fig. 6 Typical schlieren images in a cycle of the longitudinal oscillation of the shock train.

supersonic inlets, isolators of scramjets, and diffusers of supersonic wind tunnels, to name a few. A more detailed description about the shock train can be found in [19].

Since the duct exit is slightly blocked (TR = 14%) prior to the flow plug motion, a shock train is observed in the combustor at the beginning of the test. The shock train exhibits remarkable oscillatory characteristics which change with the increase of TR. Figure 4 presents the pressure-time histories of C9, C10, and C11 around the start moment of the plug motion. Figure 5 gives the joint time-frequency analysis result of the pressure signal of C11. In Fig. 5 the color represents the mean squared amplitude of power spectral density. During the analysis process, the running average is subtracted from the original pressure signal to obtain a zero-mean signal, and then wavelet transform of the zero-mean signal is performed with Morlet wavelet of which the wave number is 23. As it can be seen, both C10 and C11 sense the periodic pressure fluctuations caused by the regular motion of the shock train. At about $t = 5780$ ms, the base frequency of the pressure signal sensed by C11 decreases from 314.6 to 256.1 Hz and the fluctuation amplitude increases to some extent, from which one can infer the change of the shock train oscillation style. At about $t = 5828$ ms, the surface pressure fluctuations in the combustor decrease substantially, and the time-averaged pressures increase gradually. That is, the oscillatory characteristics of the shock train vanish.

The observation of the corresponding schlieren images confirms the preceding conjecture. The shock train oscillates with a relatively low-amplitude along the streamwise direction before $t = 5780$ ms. However, at the period of $t = 5780$–5828 ms, transverse flutter with high-amplitude dominates the oscillatory motion of the shock train. For both oscillations, the interaction of the shock train and the shear layer of the backstep flow plays the role of instability source.

Figure 6 presents schlieren images of typical moments in a cycle of longitudinal oscillation. The corresponding distributions of surface pressures are shown in Fig. 7. Because of the acceleration of the expansion fan near the backstep, the upstream Mach number of the shock train is fairly high (about 3.0). Thus an oblique shock train is observed in the combustor, of which the supersonic core flow deflects to the bottom surface all the time. The shock train oscillates as a unit in upstream-downstream direction, and the shear layer of the backstep flow is periodically raised while the shock train is at its most upstream position. This process can be explained more detailedly as follows. Initially ($t = 5711$ ms), the shear layer of the backstep flow reattaches to the bottom surface fully, and the first shock of the shock train, which is rather close to the reattachment point of the shear layer, appears immediately upstream of C10. Then, as a result of the disturbance of the initial pressure rise of the shock train, the shear layer is slightly raised and the expansion fan emanating from the corner of the backstep is hereby weakened. Since the pressure immediately upstream of the shock train increases and the pressure at the duct exit remains nearly unchanged, the required pressure rise across the shock train decreases, leading to a rapid retreat of the shock train ($t = 5712$ ms). The retreat of the shock train decreases the adverse pressure gradient near the reattachment point, thus the shear layer moves towards the bottom surface again due to its strong tendency towards reattachment. As a result, the required pressure rise across the shock train increases and it begins to move upstream ($t = 5713$ ms). At $t = 5714$ ms, the shear layer reattaches to the bottom surface fully and the shock train reaches its most upstream position, indicating the beginning of the next cycle. From the preceding description, it can also be found that the first bifurcated shock of the shock train happens to sweep C10 frequently, therefore the pressure signal of C10 fluctuates periodically and remarkably with an fluctuation amplitude of $10 \cdot p_0$. As to C11, the pressure fluctuation is much smaller due to the absence of shock sweeping and

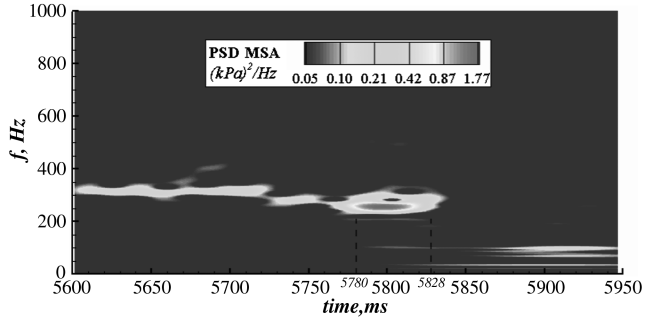

Fig. 5 Power spectrum density contours of the pressure signal of C11 at the stage of shock train in the combustor.

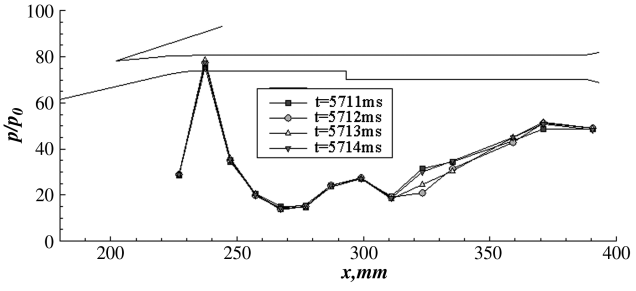

Fig. 7 Typical surface pressure distributions in a cycle of the longitudinal oscillation of the shock train.

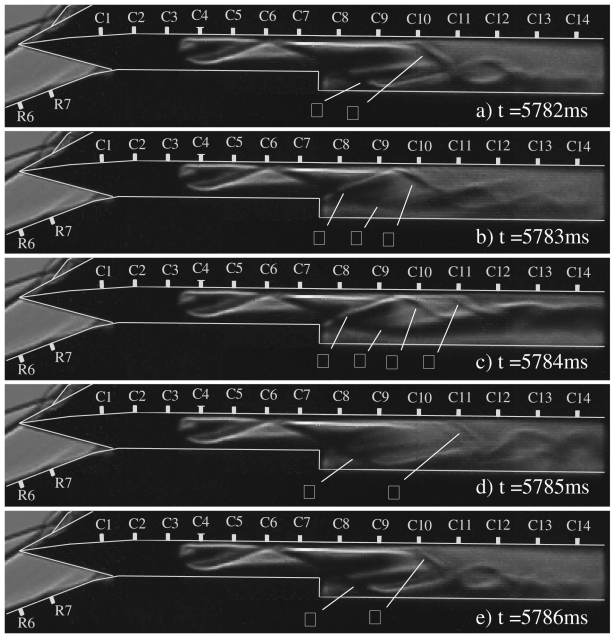

Fig. 8 Typical schlieren images in a cycle of the transverse oscillation of the shock train.

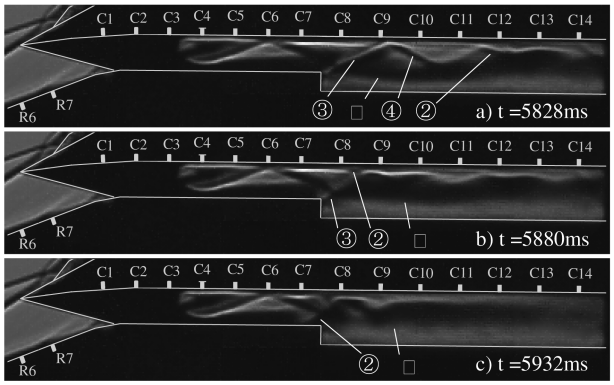

Fig. 9 Typical schlieren images of the stable propagation of shock train in the combustor.

the buffering effect of the large separation region in the shock train (Fig. 6).

Figure 8 exhibits typical schlieren images of the transverse oscillation of the shock train. As it can be seen, the interaction of the shock train and the shear layer of the backstep flow is still the inducing factor of the oscillation. What's different here is that the shear layer of the backstep flow is raised sufficiently to detach the supersonic core flow of the shock train from the bottom surface periodically, resulting in a transverse flutter of the shock train. Because the flutter involves large-scale motions of the shocks and the shear layer, the base frequency of the transverse oscillation decreases to some extent as compared with that of the longitudinal oscillation. In fact, the transverse flutter of the shock train is mixed with longitudinal oscillation. In a typical cycle, the fluctuation amplitude of the first shock position of the shock train reaches 12 mm (about 0.7 times of local duct height). In addition, since C10 and C11 are swept frequently by the first shock of the shock train, and are also disturbed by the corner expansion fan and the shear layer induced shock of which the strength changes from moment to moment, the sensed pressure fluctuations increase substantially, reaching $20 \cdot p_0$ or more.

With the upstream movement of the flow plug, the adverse pressure gradient near the backstep increases continuously. Therefore, the reattachment tendency of the shear layer decreases gradually and the amplitude of the transverse flutter descends. Finally, the supersonic core flow of the shock train does not attach to the bottom surface any more and the internal flow pattern begins to develop into a stable state. After $t = 5828$ ms, the oscillatory characteristics of the shock train diminish basically. The shock train moves towards the isolator in a steady manner. Typical schlieren images of the stable propagation of the shock train are presented in Fig. 9 and the corresponding pressure distributions are shown in Fig. 10. As it can be seen, the shear layer of the backstep flow extends to the duct exit directly. That is, the shock train develops and propagates in a channel with a solid surface at the top side and a free shear layer at the bottom side. Since the shear layer can not resist a large adverse pressure gradient, the shocks in the shock train become obscure and the streamwise pressure gradient decreases to some extent. At $t = 5828$ ms, an oblique shock is induced at the leading edge of the shear layer, which impinges on the top surface immediately downstream of C9 and leads to a reflected shock. The induced shock accomplishes a portion of the pressure gain which was originally performed by the shock train, thus the leading edge of the shock train retreats to the position between C11 and C12. Thereafter, with the movement of the flow plug, the shock train propagates upstream gradually and the inclined angle of the induced shock increases continuously. At $t = 5880$ ms, the induced shock is merged into the first bifurcated shock of the shock train. At about 5932 ms, the lower part of the first shock of the shock train goes into the isolator, indicating the end of the stage of shock train in the combustor.

B. Shock Train in the Isolator ($t = 5932$–6064 ms)

The stage of shock train in the isolator begins at $t = 5932$ ms and ends at $t = 6064$ ms. According to the schlieren images and the pressure-time histories, although some oscillations do exist while the shock train originates from the isolator, the oscillatory amplitude is rather small. For examples, the fluctuation amplitude of the first shock position is about 0.2 times the isolator height, and the root mean square value of typical pressure signals is about $4 \cdot p_0$. The fluctuation energy distribution of the instantaneous pressures is rather dispersed in the frequency domain, covering the frequency region from several hundreds Hz to about 2500 Hz (Fig. 11).

Figure 12 gives typical schlieren images while the shock train propagates in the isolator. The corresponding pressure distributions are shown in Fig. 13. Again an oblique shock train is observed in the isolator. Although the boundary layer near the bottom surface is much thicker than that near the top surface at the entrance of the isolator, the supersonic core flow of the shock train is found to deflect towards the bottom surface all the time. This is mainly resulted from the strong asymmetric interference of the reflected shock of the cowl-induced shock and the corner expansion fan around the inlet throat. The leading edge of the shock train moves near C6 at 5963 ms, near C5 at 6013 ms, and near C4 at 6063 ms. For the absence of the interference of the shear layer of the backstep flow, the shocks of the shock train become clearer and the sustainable pressure gradient becomes larger. When the leading edge of the shock train is near C4,

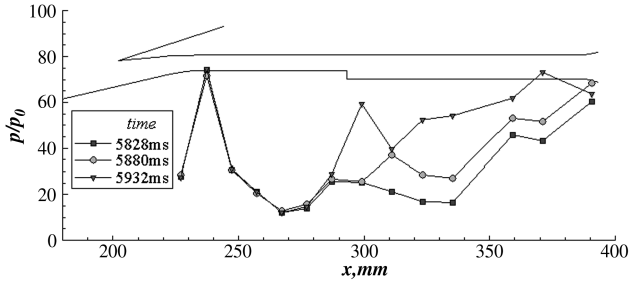

Fig. 10 Typical pressure distributions of the stable propagation of shock train in the combustor.

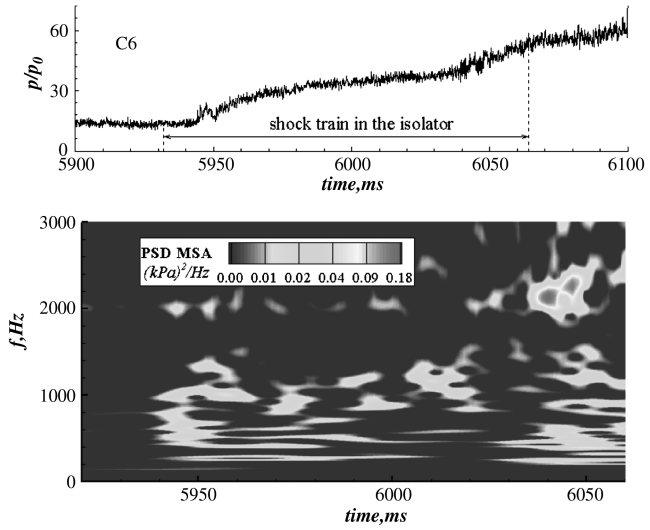

Fig. 11 Pressure-time history of C6 and the corresponding power spectrum density contour.

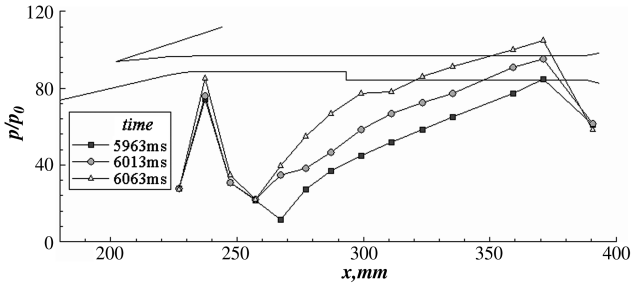

Fig. 13 Typical surface pressure distributions of the stage of shock train in the isolator.

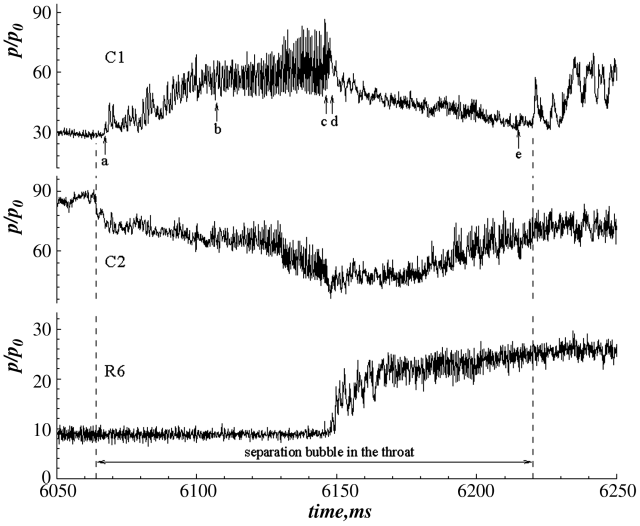

Fig. 14 Pressure-time histories of C1, C2 and R6 of the stage of separation bubble in the throat.

the first four shocks are all discriminable. Since the violent pressure fluctuations of the core flow can be well buffered by the large separation region above, all the pressure distributions shown in Fig. 13 increase smoothly along the top surface. While the shock train originates near C4, the maximum surface pressure in the duct is as high as $104.5 \cdot p_0$, and the static pressure ratio across the shock train is 4.7, of which 69% is accomplished in the isolator.

C. Separation Bubble in the Throat ($t = 6064$–6220 ms)

While the shock train originates near C4, a small upstream movement of the flow plug brings substantial changes to the pressure signals of C1 and C2 which are formerly rather stable (Fig. 14), indicating the onset of the stage of separation bubble in the throat. In the entire stage, the time-averaged pressure of C1 decreases at first and then increases, and the trend of C2 is on the contrary. The joint time-frequency analysis of these pressure signals is conducted and the obtained results are shown in Fig. 15. Taking the time-frequency characteristics of the pressure signal of C1 for example, the fluctuation energy is distributed in the frequency region from 500 to 1500 Hz at the initial part of this stage. The fluctuation energy begins to converge toward the high-frequency region (above 1500 Hz) since $t = 6107$ ms (marked with b in Fig. 14). One prominent peak frequency appears and increases with the movement of the flow plug. At 6146 ms (marked with c in Fig. 14), the peak frequency reaches 1820 Hz and the pressure fluctuation amplitude reaches $30 \cdot p_0$. However, the high-frequency fluctuation of the pressure signal diminishes after $t = 6146$ ms. The fluctuation energy drops

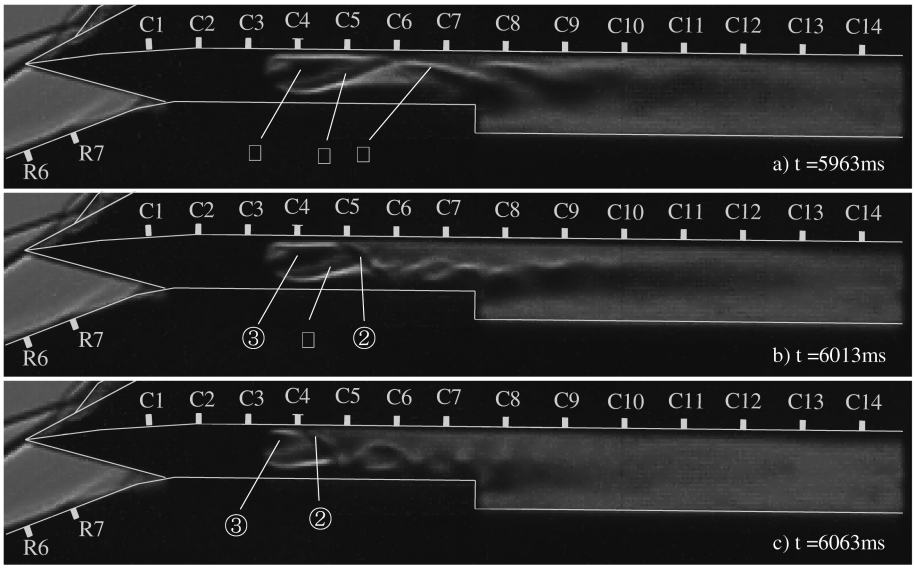

① reflected shock of the cowl induced shock; ② first shock of the shock train;

③ expansion fan near the inlet throat

Fig. 12 Typical schlieren images of the stage of shock train in the isolator.

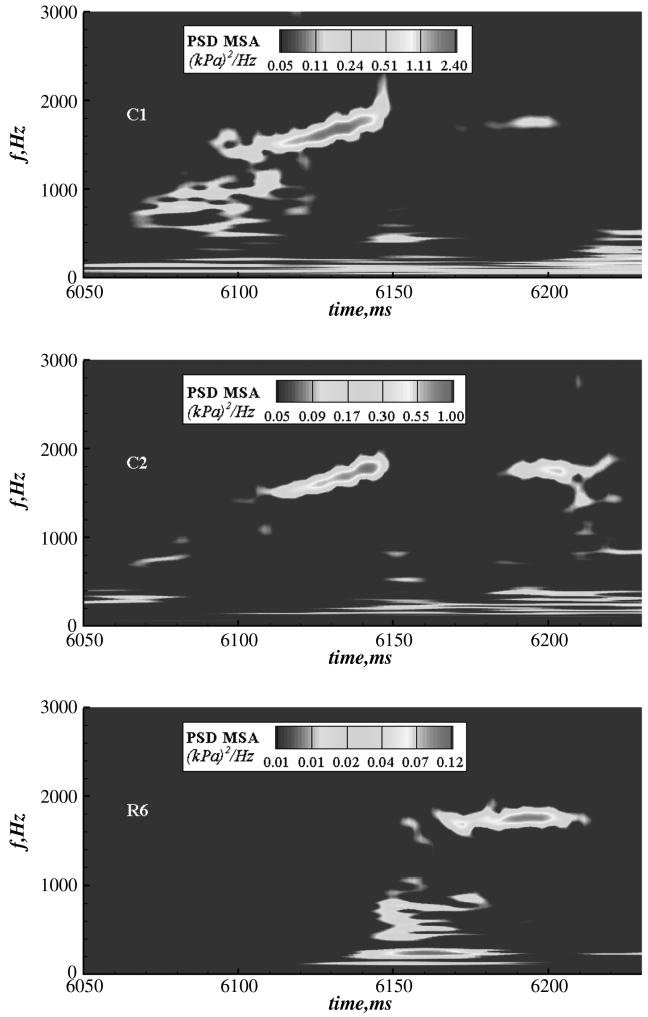

Fig. 15 Power spectrum density contours of C1, C2 and R6 of the stage of separation bubble in the throat.

substantially and shifts to the frequency region below 600 Hz. The time-frequency characteristics of the pressure signal of C2 are similar to those of C1, but the fluctuation energy is obviously lower. In addition, sensor R6, which is placed near the end of the second ramp, senses remarkable pressure fluctuations of which the fluctuation energy is distributed below 1000 Hz before 6164 ms. After $t = 6164$ ms, most of the fluctuation energy is transferred to the frequency region around 1750 Hz rapidly, indicating the reappearance of the high-frequency fluctuations which disappear from the visual field of C1. At 6213 ms, the high-frequency pressure fluctuations of R6 disappear again.

The preceding mentioned changes of the dynamic pressure characteristics will be explained according to the evolution of unsteady flow patterns in the following text. The schlieren images of typical moments marked in Fig. 14 are shown in Fig. 16. By putting the schlieren images of $t = 6067$ ms in Fig. 16 and $t = 6063$ ms in Fig. 12 together, one can notice that the corner expansion fan near the inlet throat in Fig. 16 shrinks substantially though the shock train still originates near C4. This is probably because that the adverse pressure gradient caused by the shock train propagates upstream through the thick boundary layer near the bottom surface, resulting in a large separation bubble near the incident point of the cowl-induced shock. The separation bubble forms an aerodynamic throat at the convergent part of the inlet, leading to the emergence of an induced oblique shock and the upstream movement of the corner expansion fan. Because of the unsteady disturbance of the shock train, the separation bubble moves upstream and downstream repeatedly and the induced shock sweeps C1 frequently. Therefore, the pressure signal of C1 takes on remarkable fluctuations and the frequency characteristics are similar to those signals measured in the shock train. No prominent peak frequency is observed. At the same time, because C2 happens to lie in the expansion fan presently, the pressure signal drops abruptly. Then, with the upstream movement of the shock train, the size of the separation bubble increases gradually and hence the strength of the induced shock and the expansion fan increase simultaneously. As a result, the time-averaged pressure of C1 increases and that of C2 decreases continuously.

At $t = 6107$ ms, the leading edge of the separation bubble approaches R7 and its size is so large that high-frequency self-sustained oscillations appear. When the separation bubble is at its minimum size, low energy flow begins to accumulate in the separation bubble and the bubble expands. The spillage of the low energy flow through two sides of the bubble increases at the same time. Once the spillage of the low energy flow exceeds that accumulated in the separation bubble, the bubble begins to shrinks. Therefore the separation bubble expands and shrinks repeatedly at a rather high base frequency (about 1500 Hz). As a result, all of the measurement points in the duct sense pressure fluctuations with the same high frequency, and the oscillatory characteristics of the shock train are now submerged by those of the separation bubble. When the plug continues to move upstream, the size of the separation bubble increases further and the side spillage increases, hence the oscillation frequency ascends gradually, reaching 1820 Hz at $t = 6146$ ms. At $t = 6148$ ms, the size of the separation bubble increases abruptly and its leading edge moves upstream of R6. Since C1 presently lies in the expansion fan of the separation bubble and is not swept by the induced shock anymore, its time-averaged pressure drops and the sensed pressure oscillations disappear abruptly though the high-frequency oscillations of the separation bubble still exist. At $t = 6164$ ms, the induced shock of the separation bubble sweeps R6 regularly, thus the fluctuation energy of the instantaneous pressure concentrates around 1750 Hz.

D. Unstart ($t > 6220$ ms)

At $t = 6220$ ms, the induced shock of the separation bubble moves upstream of the cowl lip for the first time, and the airflow capture characteristic of the inlet is changed. That is, the inlet enters an unstarted state. A combined analysis of the schlieren images and the pressure signals indicates that in the period of $t = 6220$–6250 ms the separation bubble at the duct entrance expands and contracts substantially, resulting in remarkable pressure fluctuations at the duct entrance (Fig. 17). The pressure fluctuation amplitudes of C1 and R5 reach $30 \cdot p_0$ and $10 \cdot p_0$, respectively, and the fluctuation energy concentrates around two peak frequencies, i.e., 150 and 230 Hz (Fig. 18). The pressure fluctuations of other measurement points are much lower. The characteristics of the preceding stated transient flows and pressures are consistent with those of little buzz as observed in [7]. Interestingly, during the period of $t = 6250$–6297 ms, both the internal and external flows of the test model are rather stable, with the entrance separation bubble being at its maximum state (Fig. 19). As shown in Fig. 19, the separation induced shock impinges near the cowl lip, and the cowl shock is detached and transformed into a bow shock. Therefore, complex shock-shock interactions appear near the cowl lip due to the intersections of the second ramp shock, the separation induced shock, and the bow shock, which lead to high local heating rates and hence increase the requirement of thermal protection. At the same time, the pressure fluctuation of each measurement point drops to a rather low level. For example, the pressure fluctuation amplitudes of C1 and R5 are presently about $10 \cdot p_0$ and $4 \cdot p_0$. This phenomenon is also observed by Wagner et al. [8] and is named as "nonoscillatory unstarted flow." This phenomenon might be explained as follows: At the non-oscillatory unstarted state, the exhaust capability of the duct is slightly smaller than that of little buzz state, thus the separation bubble expands to increase the side spillage for the mass flow balance of the duct. What's more, the induced shock of the separation bubble detaches the cowl shock and brings on additional spillage above the cowl. As a result, the spillage at the duct entrance reaches to such a state that it can be regulated smoothly only by the separation bubble size, without remarkable flow pattern change. Therefore, any

Fig. 16 Typical schlieren images of the stage of separation bubble in the throat.

disturbance originated in the duct and the caused mass flow imbalance can be damped by the separation bubble, and a quasi stable flow is formed.

After $t = 6297$ ms, the spillage above the cowl and at two sides of the duct entrance can not compensate for the decrease of the exhaust capability of the duct exit any more, the quasi stable flow in the test model is destroyed again, and the high-amplitude oscillatory flow which is called big buzz in [7] emerges. During a big buzz cycle, the transient flow pattern changes violently with time. For example, the ramp shock system is destroyed and then reestablished, the entrance separation bubble is disgorged and then swallowed, and the shock train in the isolator is developed and then dispelled by the entirely reversed flow. As to the pressure signals, the fluctuation amplitudes in the duct can reach as high as $70 \cdot p_0$. After $t = 6297$ ms, the base frequency of big buzz, around which most of the fluctuation energy concentrates, can be observed all the time (Fig. 18). At the early stage of big buzz, the base frequency shows an increasing tendency, with an initial value of 210 Hz. This tendency slows down at about $t = 6450$ ms and gives a value of 330 Hz at $t = 6530$ ms. Then, the base frequency fluctuates around 330 Hz during the following 270 ms, despite that the TR of the duct exit still keeps increasing continuously. In addition, another energy-containing frequency region which is caused by the second harmonic wave can also be clearly observed in Fig. 18.

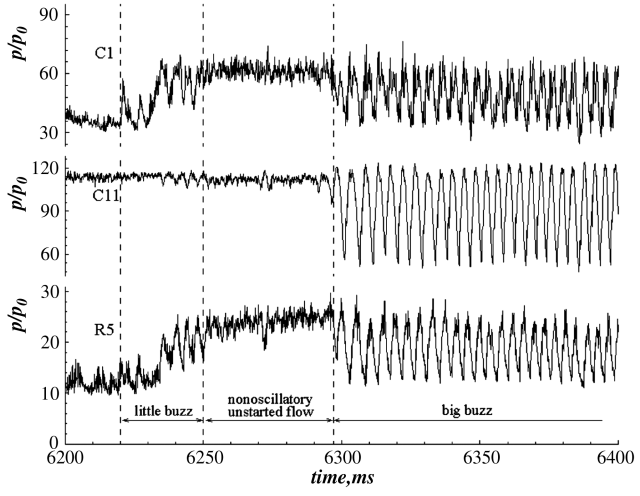

Fig. 17 Pressure-time histories of C1, C11 and R5 of the unstarted flows.

V. Discussions on the Detection and Prediction of Hypersonic Inlet Unstart

From the unsteady flow patterns and the surface pressures during the unstart process of a generic hypersonic inlet, it can be seen that the unstart process is rather complex and contains several types of

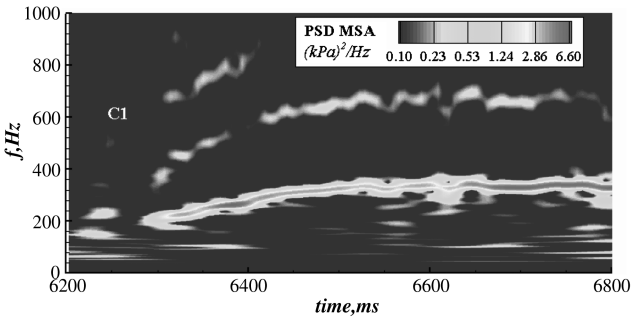

Fig. 18 Power spectrum density contours of C1 at the stage of unstart.

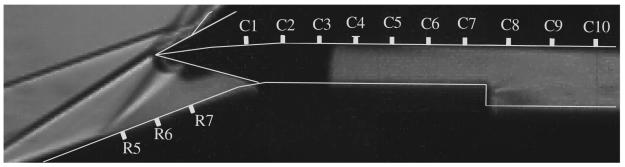

a) T =6251ms

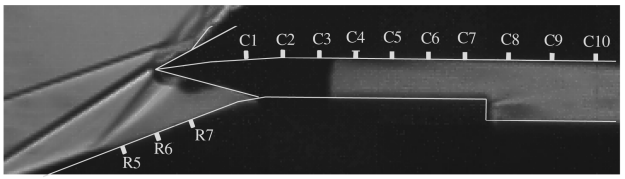

b) T =6287ms

Fig. 19 Separation bubble at the duct entrance of the nonoscillatory unstarted flow.

oscillations of different amplitudes and different dominant frequencies. Thus, it is a difficult task to identify each flow type of the unstart process by analyzing the instantaneous pressure signals. In practice, scramjets and hypersonic vehicles are mainly concerned with the detection and prediction of the unstarted flows. Hence, some discussions are made about this specific issue according to present results. At present, two theories are available for the detection and prediction of the unstart phenomenon, namely, the pattern recognition theory and the change-detection theory. In various change-detection algorithms, such as the cumulative sum algorithm, the generalized likelihood ratio algorithm, etc., there is a need to set an artificial threshold to detect the change or give the alarm [18]. The threshold will vary with the flight Mach number, the flight altitude, etc., and will need adjustments for different inlets. Therefore, a universal detection criterion for unstart can hardly be established by the change-detection theory. The following discussions are made on the assumption that a pattern recognition algorithm is used for the detection and prediction of unstart.

A. Arrangement of the Dynamic Pressure Sensors

For the present experiments, more than 20 sensors are used. While in the practical monitoring system of a hypersonic inlet, only one or two sensors can be used. Thus the sensors should be arranged carefully to reflect the changes of the inlet operating state simultaneously and sensitively. According to the current experiment, the pressure signal obtained by C1 contains abundant time-frequency characteristics, thus it can be gainfully used to discern the stages of separation bubble in the throat, little buzz, and big buzz distinctly. In other words, the first sensor should be placed at the end of the contract part and on the central line of the top surface. The second sensor, if available, can be used to monitor the status of the shock train in the isolator. In the current experiment, the supersonic core flow of the shock train deflects to the bottom surface of the isolator all the while. To capture the dynamic characteristics of the shock train clearly, the second sensor should be placed at the rear part of the isolator and on the central line of the bottom surface.

B. Extraction of the Characteristics for Different Flows

While the inlet operates at the stages of separation bubble in the throat, little buzz, or big buzz, the time-averaged pressure of C1 shifts, and the instantaneous pressure of C1 fluctuates with a prominent peak frequency. These features can be used to identify the operating status of inlet. Concretely speaking, the time-frequency features, such as time-averaged value, root mean square value, instantaneous peak frequency, measure of skewness, kurtosis, etc., can be calculated for each flow. Then, making use of relevant theories, such as Shannon information entropy method, principle component analysis method, support vector machine algorithm, etc., selection and combination of these features could be performed to ensure their stability, sensitivity, and effectivity.

C. Construction of the Classifier

Utilizing the selected or newly generated features, the classifier for inlet operating states can be constructed according to relevant criteria, such as least mean square criterion, Fisher linear discriminant, and, etc. Obviously, the classifier will report the onset of unstart if little buzz flow or big buzz flow is detected. What is more, since the stage of separation bubble in the throat is the inevitable course prior to the inlet unstart, the classifier can immediately alarm that the inlet will soon enter the unstarted status once this specific flow is detected. According to the current experiment, the alarm can possibly be given about 100 ms prior to the onset of unstart. There is still another problem worthy of special attention. To avoid wrong recognition caused by external interfering signals, the base frequencies of the separation bubble flow, little buzz flow, and big buzz flow should be introduced into the classifier. These base frequencies can be easily obtained from such wind tunnel tests. Corrections are required to take into account the influences of the model scale and the total temperature of the coming flow. As to the nonoscillatory unstarted flow, there is no obvious characteristic in the frequency domain, and thus its recognition mainly depends on the relation of time-averaged pressures, of which the accuracy and the universality can not be guaranteed.

VI. Conclusions

To provide information for the detection, prediction, and control of the inlet unstart, the present paper involves experimental investigations of the entire process from a started status to an unstarted status for a generic two-dimensional hypersonic inlet. The test model consists of an inlet, an isolator, and a dump combustor. The experiment is carried out at a free stream Mach number of 5.0. During the test, a flow plug, driven by a linear electric motor, moves upstream continuously at the duct exit and forms a gradually increasing TR downstream of the inlet. The unstart process caused by excessive heat release in the combustor is thus simulated. Simultaneous high-speed schlieren imaging and dynamic surface pressure measurements are used to record the flow structures and the surface pressures of the unstart process.

During the unstart process, both the internal/external flows and the surface pressures of the test model experience complex changes. While the shock train is contained in the combustor, its supersonic core flow deflects towards the bottom surface and oscillates streamwise at a base frequency of 314.6 Hz, causing the pressure signal of C10 fluctuates with an amplitude of $10 \cdot p_0$. Then the supersonic core flow detaches from the bottom surface periodically and leads to the transverse oscillation of the shock train with a base frequency of 256.1 Hz. The pressure fluctuation amplitude of C10 reaches $20 \cdot p_0$. Further, the shock train propagates upstream stably in the combustor, and no evident oscillation is observed. When the shock train enters the isolator, it oscillates slightly and causes wideband pressure fluctuations of which the typical amplitude is around $4 \cdot p_0$. Separation bubble appears near the inlet throat abruptly while the leading edge of the shock train arrives at C4. The dynamic characteristics of the separation bubble are initially controlled by the shock train, and the fluctuation energy is dispersed in the wide frequency range of 500–1500 Hz. While the leading edge of the separation bubble moves near R7, the high-frequency expansion and contraction of the separation bubble dominate the unsteady flow in the duct. The pressure fluctuation amplitude of C1 reaches $30 \cdot p_0$ and a prominent peak frequency, which increases with the plug movement, is observed in the range of 1500–1820 Hz. The inlet unstart occurs while the induced shock of the separation bubble goes upstream of the cowl lip for the first time. Little buzz, which is characterized by high-amplitude oscillations of the separation bubble, appears at first. The corresponding pressure fluctuation amplitudes of C1 are about $30 \cdot p_0$ and two peak frequencies are observed around 150 and 230 Hz, respectively. For the succeeding period which lasts about 50 ms, both the separation bubble and the surface pressures are temporarily stable. At last, big buzz takes place. Both the internal and external flows oscillate violently. The pressure fluctuation amplitude in the duct reaches as

high as $70 \cdot p_0$. A prominent peak frequency which increases with the plug movement is observed in the range of 210–330 Hz.

The pressure signal of C1 depicts the unsteady behaviors of the separation bubble flow, little buzz flow, and big buzz flow clearly. Therefore, using a sensor located at C1 could be a good choice for a practical inlet-status-monitoring system.

Acknowledgment

This work was supported by National Nature Science Foundation of the People's Republic of China through Grant Nos. 90916014 and 50776044.

References

[1] Curran, E. T., and Murthy, S. N. B., *Scramjet Propulsion*, Vol. 189, Progress in Astronautics and Aeronautics, AIAA, Reston, VA, 2001, pp. 462–466.

[2] McClinton, C. R., and Hunt, J. L., "Airbreathing Hypersonic Technology Vision Vehicles and Development Dreams," AIAA Paper 1999-4987, 1999.

[3] Tan, H. J., and Guo, R. W., "Experimental Study of the Unstable-Unstarted Condition of a Hypersonic Inlet at Mach 6," *Journal of Propulsion and Power*, Vol. 23, No. 4, 2007, pp. 783–788. doi:10.2514/1.28039

[4] Sun, S., Zhang, H. Y., Cheng, K. M., and Wu, Y. Z., "The Full Flowpath Analysis of a Hypersonic Vehicle," *Chinese Journal of Aeronautics*, Vol. 20, No. 5, 2007, pp. 385–393. doi:10.1016/S1000-9361(07)60059-4

[5] Voland, R. T., Auslender, A. H., and Smart, M. K., "CIAM/NASA Mach 6.5 Scramjet Flight and Ground Test," AIAA Paper 1999-4848, 1999.

[6] Walker, S., Rodgers, F., Paull, A., and Van Wie, D. M., "HyCAUSE Flight Test Program," AIAA Paper 2008-2580, 2008.

[7] Tan, H. J., Sun, S., and Yin, Z. L., "Oscillatory Flows of Rectangular Hypersonic Inlet Unstart Caused by Downstream Mass-Flow Choking," *Journal of Propulsion and Power*, Vol. 25, No. 1, 2009, pp. 138–147. doi:10.2514/1.37914

[8] Wagner, J. L., Valdivia, A., Clemens, N. T., and Dolling, D. S., "Experimental Investigation of Unstart in an Inlet/Isolator Model in Mach 5 Flow," *AIAA Journal*, Vol. 47, No. 6, 2009, pp. 1528–1542. doi:10.2514/1.40966

[9] Yu, D. R., Chang, J. T., Bao, W., and Xie, Z. X., "Optimal Classification Criterions of Hypersonic Inlet Start/Unstart," *Journal of Propulsion and Power*, Vol. 23, No. 2, 2007, pp. 310–316. doi:10.2514/1.24640

[10] Ferri, A., and Nucci, L. M., "The Origin of Aerodynamic Instability of Supersonic Inlets at Subcritical Conditions," NACA RM L50K30, 1951.

[11] Newsome, R. W., "Numerical Simulation of Near-Critical and Unsteady, Subcritical Inlet Flow," *AIAA Journal*, Vol. 22, No. 10, 1984, pp. 1375–1379. doi:10.2514/3.48577

[12] Lu, P. J., and Jain, L. T., "Numerical Investigation of Inlet Buzz Flow," *Journal of Propulsion and Power*, Vol. 14, No. 1, 1998, pp. 90–100. doi:10.2514/2.5254

[13] Trapier, S., Duveau, P., and Deck, S., "Experimental Study of Supersonic Inlet Buzz," *AIAA Journal*, Vol. 44, No. 10, 2006, pp. 2354–2365. doi:10.2514/1.20451

[14] Scott, D. H., "Wind-Tunnel Blockage and Actuation Systems Test of a Two-Dimensional Scramjet Inlet Unstart Model at Mach 6," NASA TM-109152, 1994.

[15] Rodi, P. E., Emamit, S., and Trexlers, C. A., "Unsteady Pressure Behavior in a Ramjet/Scramjet Inlet," *Journal of Propulsion and Power*, Vol. 12, No. 3, 1996, pp. 486–493. doi:10.2514/3.24061

[16] Shimura, T., Mitani, T., Sakuranaka, N., and Izumikawa, M., "Load Oscillations Caused by Unstart of Hypersonic Wind Tunnels and Engines," *Journal of Propulsion and Power*, Vol. 14, No. 3, 1998, pp. 348–353. doi:10.2514/2.5287

[17] Hawkins, W. R., and Marquart, E. J., "Two-Dimensional Generic Inlet Unstart Detection at Mach 2.5–5.0," AIAA Paper 1995-6019, 1995.

[18] Trapier, S., Deck, S., and Duveau, P., "Time-Frequency Analysis and Detection of Supersonic Inlet Buzz," *AIAA Journal*, Vol. 45, No. 9, 2007, pp. 2273–2284. doi:10.2514/1.29196

[19] Matsuo, K., Miyazato, Y., and Kim, H. D., "Shock Train and Pseudo-Shock Phenomena in Internal Gas Flows," *Progress in Aerospace Sciences*, Vol. 35, No. 1, 1999, pp. 33–100. doi:10.1016/S0376-0421(98)00011-6

N. Chokani
Associate Editor